

Network pharmacology and in vitro experiments reveal the autophagy mechanism of Yanggan-Yishui granules in improving hypertensive renal injury

Keywords

Autophagy, Network pharmacology, PI3K/AKT/mTOR signaling pathway, Hypertensive renal impairment

Abstract

Introduction

In China, Yanggan-Yishui granules (YGYSG) have been used to treat hypertensive renal damage (HRD) for over 20 years. Network pharmacology was used to determine whether YGYSG affects HRD via the autophagy pathway, which was verified using in vitro experiments.

Material and methods

Common targets of YGYSG, HRD, and the autophagy pathway were screened using network pharmacology, and effective compounds, core targets, and signaling pathways were identified. The affinity of the compounds for the core targets was evaluated using molecular docking simulations. Angiotensin II (Ang II) was used to generate an in vitro renal podocyte model using MPC-5 cells. Morphological changes in the autophagosomes were observed using transmission electron microscopy (TEM). The expression levels of autophagy-related and pathway proteins were detected using western blotting and reverse transcription quantitative real-time PCR (PCR).

Results

Network pharmacology and molecular docking analyses identified eight autophagy-related core targets and ten core components in the YGYSG treatment of HRD. These targets are mainly involved in the phosphoinositide 3-kinase (PI3K)/protein kinase B (AKT)/mammalian target of rapamycin (mTOR) signaling pathway and autophagy-related biological processes. In vitro experiments showed that Ang II-stimulated renal podocytes exhibited abnormal autophagy, and YGYSG protected renal podocytes from abnormal autophagy. In addition, YGYSG reversed abnormal autophagy and improved HRD by activating the PI3K/AKT/mTOR signaling pathway.

Conclusions

YGYSG may regulate abnormal autophagy in renal podocytes by activating the PI3K/AKT/mTOR signaling pathway and may play a role in improving HRD.

Network pharmacology and in vitro experiments reveal the autophagy mechanism of Yanggan-Yishui granules in improving hypertensive renal injury

Pan Liu^{1,2}, Tairan Hu³, Bing Gao¹, Ran Xia¹, Xiaohua Dai^{3*}, Jing Wang^{1*}

¹Research Institute of Acupuncture and Meridian, Anhui University of Chinese Medicine, Qianjiang Road, Yaohai District, Hefei 230012, Anhui, PR China

²Department of Emergency or ICU, Anhui Provincial Hospital of Integrated Traditional and Western Medicine, Qingyang Road, Shushan District, Hefei 230031, Anhui, PR China

³The First Affiliated Hospital of Anhui University of Traditional Chinese Medicine, Branch Center of the National Clinical Research Center for Cardiovascular Disease, Cardiovascular Institute of Anhui Academy of Chinese Medicine, 117 Meishan Road, Shushan District, Hefei 230031, Anhui, PR China

***Corresponding author**

Jing Wang

Research Institute of Acupuncture and Meridian, Anhui University of Chinese Medicine, Qianjiang Road, Yaohai District, Hefei 230012, Anhui, PR China

E-mail: wangjing2161@126.com

Xiaohua Dai

The First Affiliated Hospital of Anhui University of Traditional Chinese Medicine,
Branch Center of the National Clinical Research Center for Cardiovascular Disease,
Cardiovascular Institute of Anhui Academy of Chinese Medicine, 117 Meishan Road,
Shushan District, Hefei 230031, Anhui, PR China

E-mail: xin_d3980@163.com

Preprint

Abstract

Context: In China, Yanggan-Yishui granules (YGYSG) have been used to treat hypertensive renal damage (HRD) for over 20 years.

Objective: Network pharmacology was used to determine whether YGYSG affects HRD via the autophagy pathway, which was verified using *in vitro* experiments.

Materials and methods: Common targets of YGYSG, HRD, and the autophagy pathway were screened using network pharmacology, and effective compounds, core targets, and signaling pathways were identified. The affinity of the compounds for the core targets was evaluated using molecular docking simulations. Angiotensin II (Ang II) was used to generate an *in vitro* renal podocyte model using MPC-5 cells.

Morphological changes in the autophagosomes were observed using transmission electron microscopy (TEM). The expression levels of autophagy-related and pathway proteins were detected using western blotting and reverse transcription quantitative real-time polymerase chain reaction (PCR).

Results: Network pharmacology and molecular docking analyses identified eight autophagy-related core targets and ten core components in the YGYSG treatment of HRD. These targets are mainly involved in the phosphoinositide 3-kinase (PI3K)/protein kinase B (AKT)/mammalian target of rapamycin (mTOR) signaling pathway and autophagy-related biological processes. *In vitro* experiments showed that Ang II-stimulated renal podocytes exhibited abnormal autophagy, and YGYSG protected renal podocytes from abnormal autophagy. In addition, YGYSG reversed

abnormal autophagy and improved HRD by activating the PI3K/AKT/mTOR signaling pathway.

Conclusion: YGYSG may regulate abnormal autophagy in renal podocytes by activating the PI3K/AKT/mTOR signaling pathway and may play a role in improving HRD.

Keywords: Hypertensive renal impairment; Network pharmacology; Autophagy; PI3K/AKT/mTOR signaling pathway

Introduction

Hypertension is an independent risk factor for several clinical diseases and a controllable indicator of disease-related mortality (Wierzejska et al. 2020). Therefore, it has been listed as a global prevention target by the World Health Organization (Burnier and Damianaki 2023). The number of people with hypertension worldwide is estimated to exceed 1.5 billion by 2025 (Forouzanfar et al. 2017). Hypertensive renal damage (HRD) is a serious complication of hypertension. Long-term hypertension leads to renal vascular endothelial injury, glomerulosclerosis, and filtered membrane podal process lesions, resulting in renal fibrosis and increased risk of end-stage renal failure (ESRD) (Hart and Bakris 2010; Yan et al. 2016; Ma et al. 2021). Therefore, it is important to effectively control HRD to delay its progression. Currently, angiotensin-converting enzyme inhibitors (ACEI), calcium channel blockers (CCBs), and diuretics are the main

drugs used in the clinical treatment of hypertension (Lu and Crowley 2018; Agita and Alsagaff 2017). However, these drugs often have use-limiting side effects, including dry cough, lower limb edema, and enhanced sympathetic activity are frequent (Zhonghua Xin Xue Guan Bing Za Zhi 2023). In addition, their effectiveness is limited. A data survey from Eastern European countries showed that after long-term antihypertensive treatment (including two or more antihypertensive drugs), only 30.8% of patients experienced effective hypertension control (Lee et al. 2023).

Owing to its long history and theoretical basis, traditional Chinese medicine (TCM) has played a significant role in the treatment of many diseases (Zhao et al. 2020; Chin 1914-1916), including hypertension (Huang et al. 2021; Li et al. 2021). Yanggan-Yishui granules (YGYSG) were developed by Professor Zhou Yixuan, a renowned TCM practitioner in Anhui Province. These granules have been used clinically for over 20 years and have shown a remarkable effect on hypertensive kidney injury (Weiping et al. 2018). Clinical studies have demonstrated that YGYSG can improve patient symptoms, reduce the excretion of urinary microalbumin associated with early hypertensive renal damage, and enhance antihypertensive effects while reducing multiple cardiovascular risk factors (Dai et al. 2017; Gu 2005). Existing research indicates that YGYSG exerts renal protective effects by inhibiting the Ang II/TRPC6/NF- κ B pathway, thereby treating early hypertensive renal damage (Shen et al. 2022). Additionally, YGYSG regulates the levels of TGF- β , PIK, and PKB in renal tissues, inhibiting early renal damage caused by hypertension (Cai et al. 2013). YGYSG is composed of six Chinese

herbs: *Salvia miltiorrhiza*, *Lycium lycii*, *Astragalus*, *Achyranthus oxideus*, *Gorgon euryale*, and *Cuscuta*. Studies have found that *S. miltiorrhiza* can regulate autophagy in podocytes through the phosphoinositide 3-kinase (PI3K)/protein kinase B (AKT)/mammalian target of rapamycin (mTOR) signaling pathway (Chen et al. 2022) and that *Astragalus* also exerts its effects by regulating inflammation and autophagy (Yang et al. 2022).

Autophagy is a biological process through which cells maintain the stability of their internal environment by degrading discarded organelles. Under physiological conditions, autophagy protects renal cells and participates in the regulation of kidney diseases (Teh et al. 2022; Ding et al. 2015). However, in long-term hypertension, excessive autophagy damages renal podocytes and blood vessels, resulting in podocyte death and accelerating the development of HRD (Dong et al. 2016; Dryer and Reiser 2010). Therefore, identifying and regulating autophagy-related targets and signaling pathways in renal podocytes is key to effective disease therapy. Currently, the activation of the renin-angiotensin-aldosterone system (RAAS) is considered the key pathogenesis of HRD. In the state of hypertension, the RAAS is activated and induces angiotensin II (Ang II) to increase blood pressure. Ang II expression is particularly evident in the kidneys; if its expression is abnormal, renal podocytes can easily be damaged (Seong et al. 2019; van Kats et al. 2001). Autophagy is closely related to Ang II activity in the kidney, and it has been found that Ang II increase can upregulate the expression of autophagy in the kidney (Yadav et al. 2010). However, the underlying mechanism

requires further investigation.

In this study, we identified possible targets and signaling pathways of YGYSG's modulation of the autophagy pathway through network pharmacological analysis. We then verified these findings using molecular docking technology and *in vitro* experiments. This provides evidence for the use of YGYSG in the treatment of HRD.

Materials and methods

Screening of YGYSG, HRD, and autophagy targets

The drug composition of YGYSG was determined using the Traditional Chinese Medicine Systems Pharmacology Database (TCMSP) platform (<https://lsp.nwu.edu.cn/tcmsp.php>) (Ru et al. 2014), and screening criteria were set as oral availability (OB) $\geq 30\%$ and drug-likeness (DL) ≥ 0.18 ; after obtaining the active ingredients, single drug targets were searched by drug MOL.ID number (Hou et al. 2022). HRD and autophagy targets were obtained from GeneCards (<https://www.genecards.org/>) and OMIM (<https://www.omim.org/>) databases, respectively. The keywords 'hypertensive renal damage and autophagy' were entered into a disease database for retrieval, and the targets obtained from the two databases were combined. Finally, target names were converted using the UniProt database (<https://www.uniprot.org>). The Venny website (<https://bioinfogp.cnb.csic.es/tools/venny/>) provides access to the active ingredients in medicines, HRD, and common autophagy targets. These proteins can be used as key targets of YGYSG to treat HRD via the modulation of autophagy.

Construction and analysis of the protein interaction network (PPI) in the treatment of

HRD using YGYSG

The common protein-protein interaction (PPI) network of YGYSG, HRD, and the autophagy pathway was constructed using the STRING platform (<https://string-db.org/>) and the species was set as *Homo sapiens*. To ensure the reliability of the study, the confidence level was set to 0.9, and the other parameters were set to their default values. Cytoscape (version 3.9.0) software was used to import the TSV files and map the protein interaction network. A topological analysis was performed on the network. The degree value represents the size and color of the target. Component-target, core component-target-disease, and YGYSG core target pathway networks were constructed.

Gene Ontology (GO) and Kyoto Encyclopedia of Genes and Genomes (KEGG)

enrichment analysis

GO and KEGG analyses were performed using the Metascape (<https://metascape.org/>) database, with a screening criterion set at $P < 0.05$. A Microscopic Letter platform (<http://www.bioinformatics.com.cn/>) was used to generate visual images.

Active ingredients-target molecular docking

For key component selection and molecular docking, the core targets of molecular

docking small-molecule composition were identified using the TCMSP (<https://old.tcm-sp-e.com/>) database and macromolecular proteins using the AlphaFold database (<https://alphafold.ebi.ac.uk/>). The protein crystal structure was dehydrated and hydrogenated using AutodockTools and the receptor structure was prepared. OpenBabel and AutoDock were used to split the small-molecule library. Docking simulations were performed using Autodock software, and the results were imported into PyMOL for visualization.

Drugs and reagents

YGYSG was provided by the Pharmacy Department of the First Affiliated Hospital of the Anhui University of Chinese Medicine. *Salvia miltiorrhiza*, *Lycium lycii*, *Astragalus*, *Achyranthus oxideus*, *Gorgon euryale*, and *Cuscuta* are Chinese herbal medicines. The granules were ground into an ultrafine powder and dissolved in a normal saline solution (PSS) to prepare a 100% stock solution (i.e., 1.0 g powder per mL of PSS). The positive control drug benazepril (10 mg) was provided by the Pharmacy Department of the First Affiliated Hospital of Anhui University of Chinese Medicine. Ang II (5 mg) was purchased from Anhui Yingmai Biological Co. Ltd (Anhui, China). Fetal bovine serum (FBS) and HyClone High Sugar Dulbecco's Modified Eagle's Medium (DMEM) were purchased from Gibco (Grand Island, NY, USA). The Cell Counting Kit-8 (CCK-8) kit was purchased from Dojindo (Tokyo, Japan), and 0.25% trypsin-ethylenediaminetetraacetic acid (EDTA), penicillin-streptomycin solution,

radioimmunoprecipitation assay (RIPA) lysate (09271919023), and anti-Beclin-1 antibody (ab62472) were purchased from Abcam (Cambridge, UK). Anti-P62 (18420-1-AP), anti-LC3 (2775S), anti-Mtor (2972s), anti-Akt (4691S), and anti-PI3K (bsm-33219M) antibodies were purchased from Cell Signaling Technology (Danvers, MA, USA). The qPCR and gDNA remover RT Master Mix (RK20403) were obtained from AbClonal (Wuhan, China), and 3-methyladenine (3-MA) was provided by Anhui (China).

Experimental animals

Thirty male Sprague–Dawley (SD) rats weighing 200–250 g were obtained from the Experimental Center of the Anhui University of Chinese Medicine. All rats were provided with food and drinking water once a day and maintained at a constant temperature of 22 ± 2 °C and a humidity of 55–60%. This study was approved by the Experimental Animal Ethics Committee of Anhui University of Traditional Chinese Medicine (AHUCM-rats-2021135).

Rat groups and preparation of YGYSG medicated serum

The rats were randomly divided into YGYS-high (YGYS-H), -medium (YGYS-M), and -low (YGYS-L) dose groups ($n \leq 10$), positive control group ($n \leq 10$), and blank group ($n \leq 10$). The YGYS-H, YGYS-M, and YGYS-L groups were administered daily doses of 0.64 g/mL, 0.32 g/mL, and 0.16 g/mL YGYS, respectively. Rats in the positive

drug group were given 0.18 mg/mL of benazepril daily via oral gavage for two weeks. Animals in the control group received saline in the same manner and on the same schedule. One hour after the last gavage, all animals were anesthetized using an intraperitoneal injection of 3.5% pentobarbital sodium (10 mL/kg) after fasting for 24 h. Blood samples from the abdominal aorta were collected at room temperature for 2 h, and the complement was inactivated at 56 °C for 30 min. Bacteria were removed by filtration twice with a 0.22 µm microporous membrane, and blood samples were then packaged, sealed, and stored in the refrigerator at -80 °C for later use.

Cell culture

MPC-5 renal podocytes were purchased from Yingmai Technology Co. Ltd. (Hefei, China). The cells were cultured in a complete medium consisting of high glucose DMEM, 10% FBS, and 1% penicillin-streptomycin in an incubator with 5% CO₂ at 37 °C. When 70-80% of the cells were fused, 0.25% EDTA/trypsin solution was added to digest the cells. After digestion, DMEM containing 10% FBS was added to terminate digestion for subculturing.

CCK-8 assay

MPC-5 cells were seeded into 96-well plates at a density of 1×10^4 cells/mL, with six wells per group. Upon reaching 70% confluence, cells were cultured for 12 hours without serum to synchronize. Except for the control group, serum media containing

YGYS-L, YGYS-M, and YGYS-H at concentrations of 5%, 10%, 15%, and 20% were added for 24 hours. After incubation, 10 μ L of CCK-8 solution was added to each well according to the manufacturer's instructions, followed by incubation for 1 hour. The absorbance of each well was measured at 490 nm.

Transmission electron microscopy (TEM)

Three groups of cells were selected for electron microscopy: blank, model, and optimal YGYSG concentration. MPC-5 cells were collected and placed in 1.5 mL of electron microscope fixative and stored in a refrigerator at 4 °C for 6 h. The electron microscope-fixing solution was removed, 1.5 mL of PBS was added and the sample was allowed to soak for 1 h. Dehydration using ethanol was performed as follows at room temperature: 30% ethanol (1.5 mL, 10 min), 50% ethanol (1.5 mL, 10 min), 70% ethanol and saturated uranium dioxycetate (1.5 mL, 3 h), 80% ethanol (1.5 mL, 10 min), 95% ethanol (1.5 mL, 15 min), and 100% ethanol (1.5 mL, 50 min); this was repeated twice. Finally, 1.5 mL propylene was added to the sample and allowed to stand for 30 min. Finally, the sample was sliced using an ultramicrotome to a thickness of 60–80 nm for observation.

Western blotting

Total protein was extracted using RIPA lysis buffer. The proteins were quantified using the bicinchoninic acid method. Sodium dodecyl sulfate-polyacrylamide gel electrophoresis (SDS-PAGE) protein loading buffer 5X was added to the collected

protein samples at a ratio of 1:4. A boiling water bath was used for 15 min to completely denature the proteins. After the sample cooled to room temperature, it was directly sampled into an SDS-PAGE gel sampling hole. We then added 5-10 μ L to each well. Electrophoresis was carried out at 80 V for approximately 1 h. The membrane was then incubated with primary antibodies at 4 $^{\circ}$ C overnight. The primary antibodies used were as follows: p62 (1:50000), beclin-1 (1:1000), LC3 (1:1000), PI3K (1:1000), AKT (1:1000), mTOR (1:1000), and β -actin (1:1000).

Reverse transcription quantitative polymerase chain reaction (RT-qPCR)

For RNA extraction, the cell precipitate was collected and 1 mL of TRIzol was added for cracking. After complete cracking, the cells were centrifuged at 12000 rpm at 4 $^{\circ}$ C for 15 min, and the supernatant was discarded. Pre-cooled 75% ethanol (1 mL) was added (anhydrous ethanol was diluted with diethyl pyrocarbonate-treated [DEPC] water). The solutions were centrifuged at 12000 rpm at 4 $^{\circ}$ C for 5 min, and the supernatant was discarded. RNA was dried at room temperature, precipitated with 20-50 μ L DEPC water, and stored at -80 $^{\circ}$ C for later use. For the reaction, the mixture was gently mixed and centrifuged in a 0.2 mL EP tube. The samples were heated at 42 $^{\circ}$ C for 2 min and immediately bathed in ice for 1 min. The EP tubes were then added to the PCR apparatus for the RT reaction. Lastly, the above reaction solution was removed and stored at -80 $^{\circ}$ C for later use.

Statistical analysis

Data were analyzed using GraphPad Prism (version 8.0.2) and SPSS (version 26.0) software. Data were expressed as mean \pm standard deviation (mean \pm SD). One-way analysis of variance was used for comparisons between groups, and the least significant difference (LSD) t-test was used for paired comparisons between groups. Statistical significance was set at $P < 0.05$.

Results

YGYSG core components act on targets of hypertensive kidney injury via the autophagy pathway

The workflow of the experiment is illustrated in Figure 1. A total of 129 effective components were obtained by retrieving the drug ingredients using the TCMSP database and setting oral bioavailability (OB) $\geq 30\%$ and drug-likeness (DL) ≥ 0.18 as likeness conditions. Of these, 57 were *S. miltiorrhiza*, 34 were *Lycium lycii*, 15 were *Astragalus likeness*, 16 were *Achyranthes sinensis*, 2 were *Gorgon euryale*, and 10 were *Cuscuta* (Figure 2). By combining the GeneCards and OMIM database results, 7097 disease targets were obtained after removing duplicates, including 7074 and 96 targets from the GeneCards and OMIM databases, respectively. By searching for 'autophagy,' 3076 targets were obtained in the GeneCards database, 29 targets were obtained in OMIM database, and 3076 autophagy genes were obtained after combining duplicate values. By screening the intersecting targets of YGYSG, autophagy, and HRD, 118 intersecting

targets were identified (Figure 3A). Ten core compounds of YGYSG used in the treatment of HRD were identified by degree screening (Table 1): quercetin, kaempferol, beta-sitosterol, stigmasterol, luteolin, isorhamnetin, tanshinone IIa, 7-O-methylisomucronulatol, baicalein, and formononetin. By referring to target mapping in TCMSP, 118 protein names were translated into official names in the UniProt database (Table 2), and drug-composition-target and drug-composition-target-disease networks were constructed (Figure 3B).

Protein interaction analysis of YGYSG in the treatment of HRD through the autophagy pathway

Protein interactions were predicted using the STRING database (<https://string-db.org/>). A total of 118 common targets obtained from the Venn diagram were imported into the database. The PPI network was constructed using Cytoscape software with 108 nodes and 982 edges (Figure 4A-4B). Finally, core targets are screened through the cytohubb plugin; betweenness (BC), closeness (CC), and degree (DC) medians were used as screening criteria (Figure 4C), and the key core targets can be found as follows: cellular tumor antigen p53 (TP53), RAC-alpha serine/threonine-protein kinase (AKT1), signal transducer and activator of the sensor transcription 3 (STAT3), transcription factor AP-1 (JUN), caspase-3 (CASP3), tumor necrosis factor (TNF), serine/threonine-protein kinase mTOR (MTOR), and epidermal growth factor receptor (MAPK1) (Figure 4D).

Enrichment analysis of YGYSG treatment of HRD through the autophagy pathway

For an enrichment analysis using the Metascape website, 118 intersection targets were imported. The results showed that 1747 targets related to biological processes (BP), 90 targets related to cell components (CC), and 141 targets related to molecular functions (MF) were selected (Figure 5A). A total of 190 KEGG samples were obtained, most of which were primarily involved in the biological processes of hormones, nitrogen compounds, autophagy, kinase binding, protein kinase binding, and transcription factor binding (Figure 5B). KEGG analysis results mainly involved the PI3K/AKT, mTOR, HIF-1, IL-17, MAPK, VEGF, autophagy-animal, T cell receptor, and NF-kappa B signaling pathways, and a drug-target-pathway network was simultaneously constructed (Figure 5C). We further analyzed the enrichment pathways of the eight core targets (Figure 6A). The results showed that the targets were mainly enriched in the PI3K/AKT, autophagy-animal, mTOR, MAPK, and TNF signaling pathways, among which the PI3K/AKT signaling pathway was the most significant (Figure 6B). Therefore, the PI3K/AKT signaling pathway was selected for further experiments.

Molecular docking

Molecular docking simulations demonstrated the affinity of core components for core targets. The top five core components of the molecular docking small-molecule selection were quercetin, kaempferol, beta-sitosterol, stigmasterol, and luteolin, whereas the core targets TP53, AKT1, mTOR, and autophagy-related proteins beclin-1, LC3, and

P62 ranked at the top in the macromolecular selection topology (Figure 7A). Quercetin, kaempferol, beta-sitosterol, stigmasterol, and luteolin exhibited good binding energies for TP53, AKT1, mTOR, beclin-1, LC3, and P62. The six groups of visual displays with the best docking results were selected (Figure 7B).

Optimal serum concentration of YGYSG

We studied the effect of different concentrations of YGYSG-mediated serum on the viability of MPC-5 cells. Cells were treated with low, medium, and high doses of YGYS-mediated serum at concentrations of 5, 10, 15, and 20% for 12, 24, and 48 h, and a CCK-8 assay was performed to calculate cell viability. Default cell viability in the control group was 100%. In the YGYS-L group, cell viability at 5% concentration after 24 h was significantly higher than that in the control group ($P < 0.01$, Figure 8A). In YGYS-M, the cell viability at 5% YGYS drug-containing serum for 12, 24, and 48 h, 10% YGYS drug-containing serum for 24 and 48 h, and 15% YGYS drug-containing serum for 24 h was significantly higher than that of the control group ($P < 0.01$, Figure 8B). In addition, compared to the 20% YGYS drug-containing serum, the 5% YGYS drug-containing serum showed significantly higher cell viability after 24 h of treatment ($P < 0.05$, Figure 8B). In the YGYS-H group, compared to the control group, the 15% YGYSG drug-containing serum showed significantly higher cell viability after 48 h of treatment ($P < 0.01$, Figure 8C). Therefore, MPC-5 cells were treated with 5% concentration of YGYS-M for 24 h for TEM. Western blotting and RT-qPCR

experiments employed 5% YGYS-L treatment of MPC-5 cells for 24 hours, 5% YGYS-M treatment of MPC-5 cells for 24 hours, and 15% YGYS-H treatment of MPC-5 cells for 48 hours.

YGYSG medicated serum inhibited autophagy of MPC-5 cells

We studied the presence of autophagic vacuoles using TEM. TEM observations showed that autophagosomes in the normal group had a normal morphology and organelle structure. Ang II-stimulated podocytes showed over-expanded autophagosomes, the number of which increased greatly, and the structure of the organelles was destroyed.

The organelles of YGYSG-treated cells appeared intact, the autophagosomes were smaller in shape and significantly reduced in number, and the double-layer membrane structure of the autophagosomes was complete (Figure 9). These morphological changes indicated that YGYSG inhibited autophagy in renal podocytes.

YGYSG inhibits autophagy of MPC-5 cells through the PI3K/AKT/mTOR signaling pathway

To explore the precise role of YGYSG-medicated serum in Ang II-induced autophagy of MPC-5 cells, western blotting and RT-qPCR were employed to measure the levels of PI3K/AKT/mTOR signaling pathway and autophagy-related markers. The results showed that, compared with the control group, the protein expression of PI3K, AKT, and beclin-1 in the model and YGYS-L groups increased ($P < 0.05$, figure 10 and figure

11) and the protein expression of LC3-II/LC3-I in the model, benazepril, YGYS-M, and YGYS-L groups increased ($P < 0.05$, figure 10 and figure 11). The expression of mTOR and p62 proteins in the model and YGYS-L groups was decreased compared to that of the control group ($P < 0.05$, figure 10 and figure 11). Compared to the model group, the protein expression of PI3K, AKT, and beclin-1 in the 3-MA, benazepril, YGYS-H, and YGYS-M groups was downregulated ($P < 0.05$, figure 10 and figure 11), whereas the protein expression of mTOR in the 3-MA, benazepril, YGYS-H, and YGYS-M groups was upregulated ($P < 0.05$, figure 10 and figure 11). The protein expression of p62 in the 3-MA and YGYS-H groups was increased, whereas that of LC3-II/LC3-I in the 3-MA and YGYS-H groups was decreased ($P < 0.05$, figure 10 and figure 11). Furthermore, the expression of mTOR protein was downregulated in the benazepril, YGYS-H, and YGYS-M groups, whereas the expression of PI3K, AKT, beclin-1, and LC3-II/LC3-I in the YGYS-L group was higher ($P < 0.05$, figure 10 and figure 11) than that in the 3-MA group.

The RT-qPCR results showed that compared to the control group, PI3K, AKT, and mTOR mRNA expression in the model, benazepril, YGYS-M, and YGYS-L groups increased ($P < 0.05$, figure 12). Compared with the model group, PI3K, AKT, and mTOR mRNA expression in the 3-MA, benazepril, YGYS-H, YGYS-M, and YGYS-L groups decreased ($P < 0.05$, figure 12). Compared to the 3-MA group, AKT and mTOR mRNA expression in the benazepril, YGYS-M, and YGYS-L groups increased ($P < 0.05$, figure 12), and PI3K mRNA expression in the YGYS-M and YGYS-L groups increased

($P < 0.05$, figure 12). To clarify the relationship between YGYS-containing serum and autophagy, we conducted a response experiment. The results showed that the protein expression level of LC3-II/LC3-I in the YGYS-M +3-MA (25 mM) group was significantly lower than that in the model group ($P < 0.05$, figure 13 and figure 14). Compared to the YGYS-M group, the protein expression level of LC3-II/LC3-I in the YGYS-M +3-MA (25 mM) group decreased significantly ($P < 0.05$, figure 13 and figure 14). These results indicated that YGYSG and autophagy have a synergistic relationship in MPC-5 cells, and YGYSG may inhibit autophagic activity by activating the PI3K/AKT/mTOR signaling pathway.

Discussion

Hypertension is a threat to global human health, and its incidence is increasing annually (Guwatudde et al. 2015). Chronic uncontrolled hypertension can also lead to kidney damage (Sun et al. 2019). Traditional Chinese medicine, which has multiple targets and fewer side effects, plays an important role in the treatment of hypertension. Previous studies have shown that YGYSG improves vascular endothelial disorders, regulates blood pressure and inflammatory responses, and improves clinical symptoms in patients with HRD (Yexiang et al. 2021).

Autophagy is the process of self-degradation of damaged organelles to maintain homeostasis in the intracellular environment (Zuo et al. 2023). Autophagy has long been considered beneficial to the body because it can help remove harmful pathogen products

and simultaneously degrade discarded organelles to produce nutrition energy (Oyagbemi et al. 2018; Zhang et al. 2023). This is most evident in the early development of tumors (Yuan et al. 2016). However, autophagy is a double-edged sword and abnormally activated autophagy can cause cell damage (Chen et al. 2013). Recent studies have shown that autophagy is involved in kidney disease and is closely related to HRD. Long-term hypertension leads to abnormal renal autophagy, an important factor in HRD progression and development (Yadav et al. 2010). In this study, the associated targets and signaling pathways of YGYSG, autophagy, and HRD were screened using network pharmacology. Network pharmacological analysis showed that the core components of YGYS used to treat hypertensive kidney injury through the autophagy pathway were quercetin, kaempferol, beta-sitosterol, stigmasterol, luteolin, isorhamnetin, tanshinone II, 7-O-methylisomucronulatol, baicalein, and formononetin. Studies have found that quercetin has physiological effects on cell apoptosis, autophagy, pyrodeath, and other cellular processes (Yadav et al. 2010) and inhibits the formation of kidney autophagosomes in mice by inhibiting oxidative stress (Yuan et al. 2016). Kaempferol can regulate beclin-1, LC3, and endoplasmic reticulum stress levels (Ashrafizadeh et al. 2020) and inhibit the autophagic activity of cells by degrading p62/SQSTM1 (Kim et al. 2018). Luteolin can reduce Ang II-induced kidney injury in HRD (Liu et al. 2021) and regulate autophagy in kidney injury by participating in the AMPK/mTOR signaling pathway (Xu et al. 2021). As a flavonoid, isorhamnetin is involved in the treatment of liver, tumors, and other diseases (Liu et al. 2019) and plays

/various inhibitory roles in autophagy (Lu et al. 2018). This suggests that our bioinformatics analysis is consistent with existing reports, indicating that YGYSG may alleviate HR by regulating cellular autophagy.

Ang II is an important activator of RAAS system, and the activation of the RAAS system plays an important role in the pathogenesis of HRD and renal autophagy. Studies have found that in patients with HRD, the concentration of Ang II in the kidney is higher than that in circulating blood (Nishiyama and Kobori 2018), and Ang II can directly act on podocytes, resulting in excessive autophagy (Lara et al. 2012); therefore, we chose Ang II for *in vitro* stimulation. Excessive autophagy induced by Ang II aggravates damage to the renal blood vessels and podocytes (Yadav et al. 2010). Our previous studies showed that YGYSG regulates Ang II levels during HRD treatment (Xiaohua and Yi 2021). TEM observations showed that Ang II-stimulated podocytes showed over-expanded autophagosomes, the number of which increased greatly, and the structure of the organelles was destroyed, as has been reported by previous authors. Notably, the number and morphology of autophagosomes in the YGYSG group were normal and the morphology of the organelles was improved. The core targets identified by the protein interaction analysis were TP53, AKT1, STAT3, JUN, CASP3, TNF, MYC, MTOR, EGFR, and MAPK1. Most of these targets are associated with inflammation and REDOX. In the state of hypertension, inflammatory products accumulate in renal vessels, and the protein expression of AKT1, STAT3, and TNF, which are important markers of hypertensive kidney injury, is upregulated (Mennuni et al. 2014).

Furthermore, we demonstrated that the HRD targets of YGYSG were mainly enriched in the PI3K/AKT/mTOR signaling pathway and mTOR signaling; therefore, we selected the PI3K/AKT/mTOR signaling pathway as the focus of further research. PI3K, a phosphatidylinositol kinase, activates the downstream target growth factor receptor (EGFR), which alters AKT protein structure. The mammalian target proteins of rapamycin (mTOR) are divided into mTOR1 and mTOR2, with mTOR1 being a key target in the regulation of autophagy (Dou et al. 2019). When the intracellular energy levels are unbalanced, PI3K/AKT and mTOR are activated, inhibiting autophagy (Ma et al. 2021). Compared to the model group, the protein expression of PI3K, AKT, beclin-1, and LC3-II/LC3-I was downregulated after YGYSG treatment, whereas the protein expression of mTOR and p62 was upregulated. These results are consistent with previous reports, indicating that YGYSG may alleviate HRD by regulating the PI3K/AKT/mTOR signaling pathway and modulating autophagy processes.

Certainly, this study has some limitations. In the cell experiment, we conducted a small response experiment to show the relationship between YGYSG and autophagy. However, the mechanism of action of YGYSG for Ang II-induced hyperautophagy in renal podocytes requires further investigation. In the future, we will verify the effect of YGYSG on the regulation of HRD through the PI3K/AKT/mTOR pathway *in vivo* and conduct further *in vitro* experiments to provide a possible basis for the treatment of HRD using traditional Chinese medicine.

Conclusion

Our results showed a synergistic relationship between YGYSG and autophagy in HRD. This study utilized network pharmacology and *in vitro* experiments to investigate the effects of YGYSG on HRD through the autophagy pathway. Network pharmacology identified key targets and compounds associated with YGYSG's action, focusing on the PI3K/AKT/mTOR signaling pathway and autophagy-related processes. *In vitro* experiments using Ang II-stimulated renal podocytes demonstrated that YGYSG exerts therapeutic effects by modulating autophagy via the PI3K/AKT/mTOR pathway in hypertensive renal damage. This study has important implications for improving outcomes in HRD research and clinical practice.

Acknowledgments

We would like to thank the platform support provided by Anhui Provincial Key Laboratory of Meridians and Organs.

Conflicts of Interest

The authors declare that the research was conducted in the absence of any commercial or financial relationships that could be construed as a potential conflict of interest.

Data availability statement

The original contributions proposed in the study are included in the article/supplementary materials, and further inquiries can be directly addressed to the corresponding author.

Author Contributions

PL: conceptualization, methodology, writing, review and editing, and approval for final version. TRH and BG: investigation, data curation, formal analysis, and approval for final version. RX: investigation, data curation, software, and approval for final version. XHD: methodology, writing review and editing, and approval for final version. WJ: conceptualization, writing, review and editing, and approval for final version. All authors contributed to the article and approved the submitted version.

Funding Statement

The present review was funded by the National Natural Science Foundation of China (81574084); and the natural science research project of colleges and universities in Anhui Province, China (kj2021a0570;2023AH050796), Xin'an Medical and Traditional Chinese Medicine Modernization Research Institute "Unveiling and Leading" Project (2023CXMMTCM022).

Consent form

All named authors have agreed to the publication of the work.

References

Agita A, Alsagaff MT. 2017. Inflammation, immunity, and hypertension. *Acta Med Indones.* 49(2):158–165.

Ashrafizadeh M, Tavakol S, Ahmadi Z, Roomiani S, Mohammadinejad R, Samarghandian S. 2020. Therapeutic effects of kaempferol affecting autophagy and endoplasmic reticulum stress. *Phytother Res.* 34(5):911–923.

Burnier M, Damianaki A. 2023. Hypertension as cardiovascular risk factor in chronic kidney disease. *Circ Res.* 132(8):1050–1063.

Cai MM, Long ZJ, Zhou YH, Ding BC, Chen C, and Lu SX. 2013. Effects of Yanggan Yishui Granules on Renal TGF- β 1, PI3K, and PKB in Spontaneously Hypertensive Rats (in Chinese), *Drug Evaluation Study.* 4

Chen J, Yuan S, Zhou J, Huang X, Wu W, Cao Y, Liu H, Hu Q, Li X, Guan X, et al. 2022. Danshen injection induces autophagy in podocytes to alleviate nephrotic syndrome via the PI3K/AKT/mTOR pathway. *Phytomedicine.* 107:154477.

Chen L, Zhang B, Toborek M. 2013. Autophagy is involved in nanoalumina-induced cerebrovascular toxicity. *Nanomed Nanotechnol Biol Med.* 9(2):212–221.

Chinese Society of Cardiology, Chinese Medical Association, Editorial Board of Chinese Journal of Cardiology. 2023. Chinese experts consensus on diagnosis and management of salt-sensitive hypertension. *Zhonghua Xin Xue Guan Bing Za Zhi.* 51(4):364–376.

Dai Xh, Xu ZJ, Qi XW, Liang CN, Wang CL, Dong M, Yang F, Wang YY, Fu J, and Yuan L. 2017. The Effects of Yanggan-Yishui Granules on Early Renal Damage in Hypertension and Multiple Cardiovascular Risk Factors (in Chinese). *J Cardiovasc Cerebrovasc Dis Integr Tradit Chin West Med.* 015: 901-04.

Ding K, Wang Y, Jiang W, Zhang Y, Yin H, Fang Z. 2015. Qian Yang yu yin granule-containing serum inhibits angiotensin II-induced proliferation, reactive oxygen species production, and inflammation in human mesangial cells via an NADPH oxidase 4-dependent pathway. *BMC Complement Altern Med.* 15:81.

Dong Q, Xing W, Fu F, Liu Z, Wang J, Liang X, Zhou X, Yang Q, Zhang W, Gao F, et al. 2016. Tetrahydroxystilbene glucoside inhibits excessive autophagy and improves microvascular endothelial dysfunction in prehypertensive spontaneously hypertensive rats. *Am J Chin Med.* 44(7):1393–1412.

Dou F, Liu Y, Liu L, Wang J, Sun T, Mu F, Guo Q, Guo C, Jia N, Liu W, et al. 2019. Aloe-emodin ameliorates renal fibrosis via inhibiting PI3K/Akt/mTOR signaling pathway in vivo and in vitro. *Rejuvenation Res.* 22(3):218–229.

Dryer SE, Reiser J. 2010. Trpc6 channels and their binding partners in podocytes: role in glomerular filtration and pathophysiology. *Am J Physiol Ren Physiol.* 299(4):F689–F701.

Forouzanfar MH, Liu P, Roth GA, Ng M, Biryukov S, Marczak L, Alexander L, Estep K, Hassen Abate K, Akinyemiju TF, et al. 2017. Global burden of hypertension and systolic blood pressure of at least 110 to 115 mm Hg, 1990–2015. *JAMA.* 317(2):165–

182.

Gu JX. 2005. Observing the Effects of Zhou's Yanggan-Yishui Granules on Alleviating Early Renal Damage in Primary Hypertension (in Chinese). *J Clin Tradit Chin Med*. 17: 373-74.

Guwatudde D, Nankya-Mutyoba J, Kalyesubula R, Laurence C, Adebamowo C, Ajayi I, Bajunirwe F, Njelekela M, Chiwanga FS, Reid T, et al. 2015. The burden of hypertension in sub-Saharan Africa: a four-country cross sectional study. *BMC Publ Health*. 15:1211.

Hart PD, Bakris GL. 2010. Hypertensive nephropathy: prevention and treatment recommendations. *Expert Opin Pharmacother*. 11(16):2675–2686.

Hou FF, Yu ZY, Cheng Y, Liu Y, Liang S, Zhang F. 2022. Deciphering the pharmacological mechanisms of *Scutellaria baicalensis* Georgi on oral leukoplakia by combining network pharmacology, molecular docking and experimental evaluations. *Phytomedicine*. 103:154195.

Huang K, Zhang P, Zhang Z, Youn JY, Wang C, Zhang H, Cai H. 2021. Traditional Chinese Medicine (TCM) in the treatment of COVID-19 and other viral infections: efficacies and mechanisms. *Pharmacol Ther*. 225:107843.

Kim CJ, Shin SH, Kim BJ, Kim CH, Kim JH, Kang HM, Park BS, Kim IR. 2018. The effects of kaempferol-inhibited autophagy on osteoclast formation. *Int J Mol Sci*. 19(1):125.

Lara LS, McCormack M, Semprum-Prieto LC, Shenouda S, Majid DS, Kobori H,

Navar LG, Prieto MC. 2012. At1 receptor-mediated augmentation of angiotensinogen, oxidative stress, and inflammation in ang ii-salt hypertension. *Am J Physiol Ren Physiol.* 302(1):F85–F94.

Lee KJ, Ryu JK, Cho YH, Shin WY, Kim JS, Yoon YW, Jang JY, Kim WH, Beom JW, Kang SM, et al. 2023. Effectiveness and safety of a fixed-dose combination of valsartan and rosuvastatin (Rovatitan® tablet) in patients with concomitant hypertension and hyperlipidemia: an observational study. *Drug Des Dev Ther.* 17:1047–1062.

Li S, Wu Z, Le W. 2021. Traditional Chinese medicine for dementia. *Alzheimers Dement.* 17(6):1066–1071.

Liu N, Feng J, Lu X, Yao Z, Liu Q, Lv Y, Han Y, Deng J, Zhou Y. 2019. Isorhamnetin inhibits liver fibrosis by reducing autophagy and inhibiting extracellular matrix formation via the TGF- β 1/Smad3 and TGF- β 1/p38 MAPK pathways. *Mediators Inflamm.* 2019:6175091.

Liu YS, Yang Q, Li S, Luo L, Liu HY, Li XY, Gao ZN. 2021. Luteolin attenuates angiotensin II-induced renal damage in apolipoprotein E-deficient mice. *Mol Med Rep.* 23(2):157.

Lu X, Crowley SD. 2018. Inflammation in salt-sensitive hypertension and renal damage. *Curr Hypertens Rep.* 20(12):103.

Lu X, Liu T, Chen K, Xia Y, Dai W, Xu S, Xu L, Wang F, Wu L, Li J, et al. 2018. Isorhamnetin: A hepatoprotective flavonoid inhibits apoptosis and autophagy via P38/PPAR- α pathway in mice. *Biomed Pharmacother.* 103:800–811.

- Ma L, Zhang R, Li D, Qiao T, Guo X. 2021. Fluoride regulates chondrocyte proliferation and autophagy via PI3K/AKT/mTOR signaling pathway. *Chem Biol Interact.* 349:109659.
- Mennuni S, Rubattu S, Pierelli G, Tocci G, Fofi C, Volpe M. 2014. Hypertension and kidneys: unraveling complex molecular mechanisms underlying hypertensive renal damage. *J Hum Hypertens.* 28(2):74–79.
- Nishiyama A, Kobori H. 2018. Independent regulation of renin-angiotensin-aldosterone system in the kidney. *Clin Exp Nephrol.* 22(6):1231–1239.
- Oyagbemi AA, Omobowale TO, Ola-Davies OE, Asenuga ER, Ajibade TO, Adejumobi OA, Arojoye OA, Afolabi JM, Ogunpolu BS, Falayi OO, et al. 2018. Quercetin attenuates hypertension induced by sodium fluoride via reduction in oxidative stress and modulation of HSP 70/ERK/PPAR γ signaling pathways. *BioFactors.* 44(5):465–479.
- Ru JL, Li P, Wang JA, Zhou W, Li BH, Huang C, Li PD, Guo ZH, Tao WY, Yang YF, et al. 2014. TCMSP: A database of systems pharmacology for drug discovery from herbal medicines. *J Cheminform.* 6:13.
- Seong SB, Ha DS, Min SY, Ha TS. 2019. Autophagy precedes apoptosis in angiotensin II-induced podocyte injury. *Cell Physiol Biochem.* 53(5):747–759.
- Shen DQ, Dai XH, Yang F, Wang YY, Shao ZB, Fu J, Ran YL, and Liang Y. 2022. Effects of Yanggan-Yishui Granules on the Ang II/TRPC6/NF- κ B Pathway in Rats with Early Hypertensive Renal Damage (in Chinese). *New Drugs Tradit Chin Med Clin Pharmacol.* 033.

Sun D, Wang JJ, Wang W, Wang J, Wang LN, Yao L, Sun YH, Li ZL. 2019. Human podocyte injury in the early course of hypertensive renal injury. *World J Clin Cases*. 7(22):3698–3710.

Teh YM, Mualif SA, Lim SK. 2022. A comprehensive insight into autophagy and its potential signaling pathways as a therapeutic target in podocyte injury. *Int J Biochem Cell Biol*. 143:106153.

van Kats JP, Schalekamp MA, Verdouw PD, Duncker DJ, Danser AH. 2001. Intrarenal angiotensin II: interstitial and cellular levels and site of production. *Kidney Int*. 60(6):2311–2317.

Weiping LI, Yunhai Z, Junhua W, et al. 2018. Treatment effect of Yanggan Yishui granule on early Renal injury in hypertension patients and the effect on blood pressure variability. *Chin Arch Trad Chin Med*. 36(08):1917–1919.

Wierzejska E., Giernaś B., Lipiak A, Karasiewicz M, Cofta M, and taszewski R. 2020. A global perspective on the costs of hypertension: a systematic review. *Arch Med Sci*. 16: 1078-91.

Xiaohua D, Yi J. 2021. Effect of Yanggan Yishui granules on plasma Ang II, AT1R Content and Renal, AT1R, TRPC6 Protein Expression in Spontaneous Hypertensive Rats[J]. *lishizhen medicine and mate ria medica reseach*. 32(08):1877–1880.

Xu X, Yu Z, Han B, Li S, Sun Y, Du Y, Wang Z, Gao D, Zhang Z. 2021. Luteolin alleviates inorganic mercury-induced kidney injury via activation of the AMPK/mTOR autophagy pathway. *J Inorg Biochem*. 224:111583.

Yadav A, Vallabu S, Arora S, Tandon P, Slahan D, Teichberg S, Singhal PC. 2010. Ang ii promotes autophagy in podocytes. *Am J Physiol Cell Physiol.* 299(2):C488–C496.

Yan SH, Zhao NW, et al. 2016. Hsp90beta is involved in the development of high salt-diet-induced nephropathy via interaction S. Ma, et al. 302 (2023) 11587815 with various signalling proteins. *Open Biol. J Ethnopharmacol.* 6:150159.

Yang Y, Hong M, Lian WW, Chen Z. 2022. Review of the pharmacological effects of astragaloside IV and its autophagic mechanism in association with inflammation. *World J Clin Cases.* 10(28):10004–10016.

Yexiang Z, Xiaoyu C, Yebin HU, et al. 2021. Effect of Yanggan Yishui granule on blood pressure variability, vascular endothelial function and urinary protein in patients with hypertension of yin deficiency Yang hyperactivity type/ZHANG Beibei. *Chin Med Innov.* 18(27):95–99.

Yuan Y, Ma S, Qi Y, Wei X, Cai H, Dong L, Lu Y, Zhang Y, Guo Q. 2016. Quercetin inhibited cadmium-induced autophagy in the mouse kidney via inhibition of oxidative stress. *J Toxicol Pathol.* 29(4):247–252.

Zhao Q, Li Y, Chen C. 2020. Current status and prospects of research on mechanism of action of traditional Chinese medicine in treating essential hypertension. *Chin J.* 1914–1916. *Tradl. China Med.* 35.

Zhang P., Liao J, Wang X, and Feng Z. 2023. High glucose promotes apoptosis and autophagy of MC3T3-E1 osteoblasts. *Arch Med Sci.* 19: 138-50.

Zuo H, Chen C, Sa Y. 2023. Therapeutic potential of autophagy in immunity and

inflammation: current and future perspectives [Published online ahead of print, 2023 Apr 29]. *Pharmacol Rep.* 75(3):499–510. 10.1007/s43440-023-00486-0.

Figure Legends

Figure 1. The workflow of the experiment.

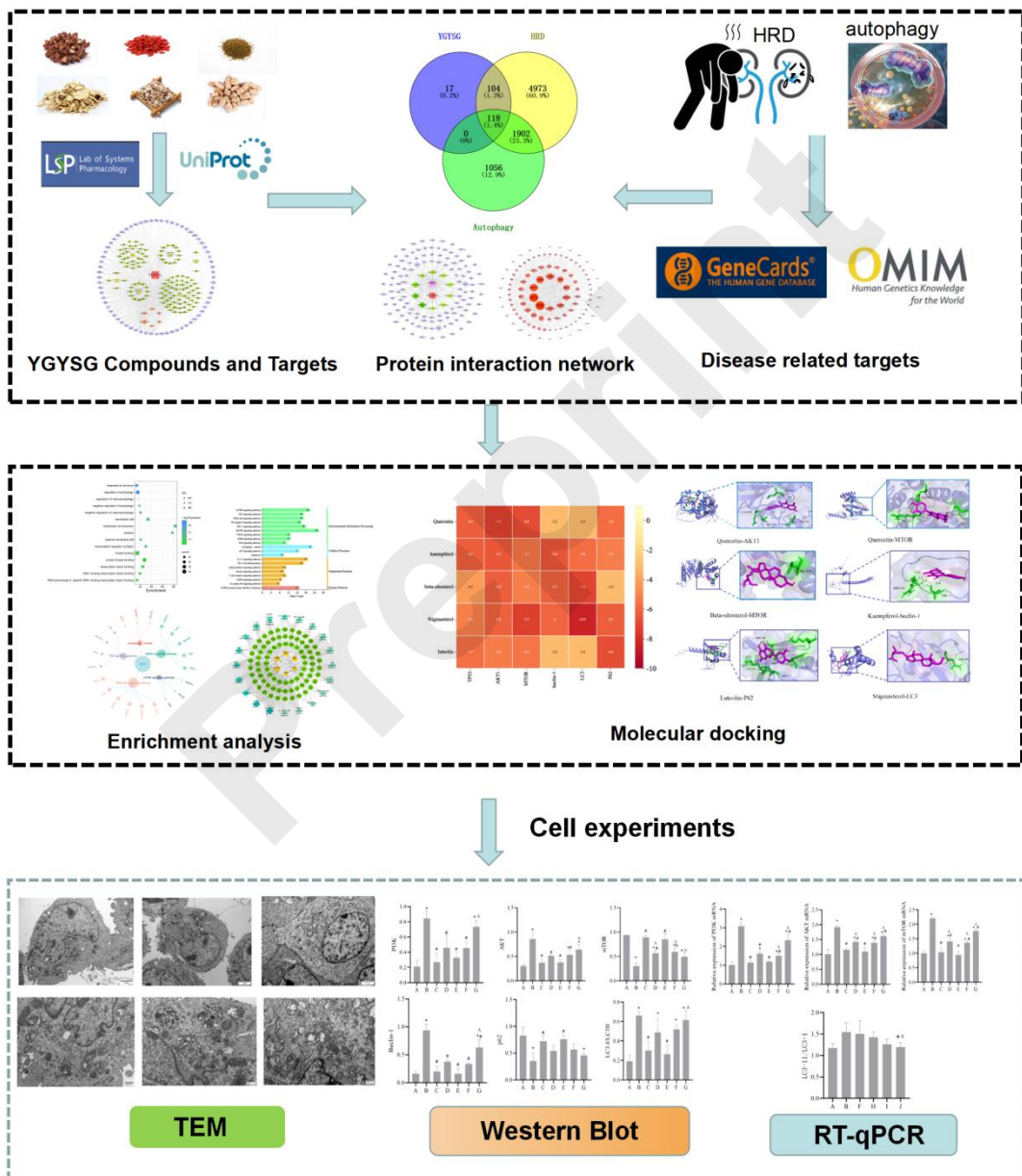


Figure 2. Construction of YGYSG component target network; the blue circle, green hexagon, pink hexagon, yellow diamond, and dark red squares represent drug target, drug component, drug common component, and traditional Chinese medicine, and YGYSG, respectively. YGYSG: Yanggan-Yishuigranules.

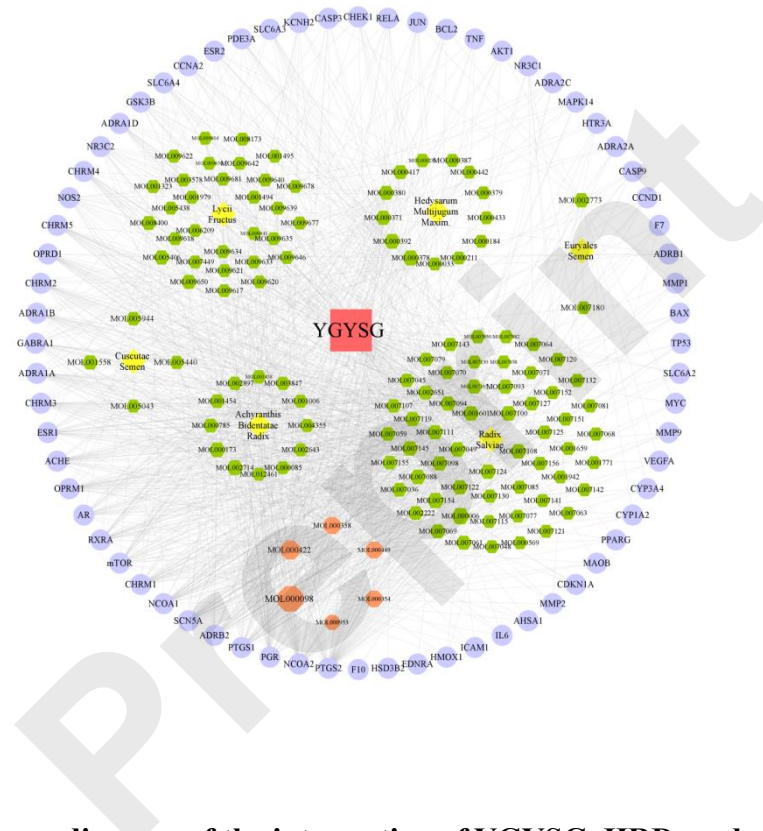


Figure 3. A: Wayne diagram of the intersection of YGYSG, HRD, and autophagy;

B: YGYSG core component target disease network construction; the blue diamond, green hexagon, red square, and purple triangle represent intersection targets, core components, drugs, and diseases, respectively. YGYSG: Yanggan-Yishui granules; HRD: hypertensive renal damage.

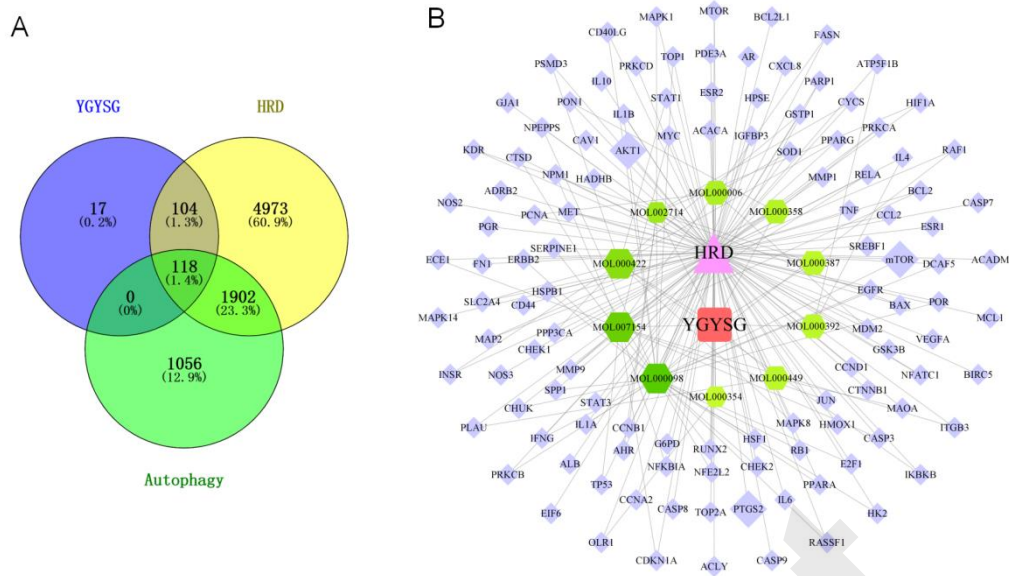


Figure 4. A: STRING PPI network obtained from the database; the highest protein interaction score was set as 0.9. B: In the PPI network constructed by cytoscape software, the size of the circle and the shade of red were positively correlated with the degree value. C: According to the cytohubb plugin, $BC \geq 0.011$ (median), $CC \geq 0.495$ (median), and $DC \geq 32$ (median) should be screened. The sector area of each target in the figure was positively correlated with the percentage. D: Wayne diagram of intersection targets of BC, CC, and DC modules.

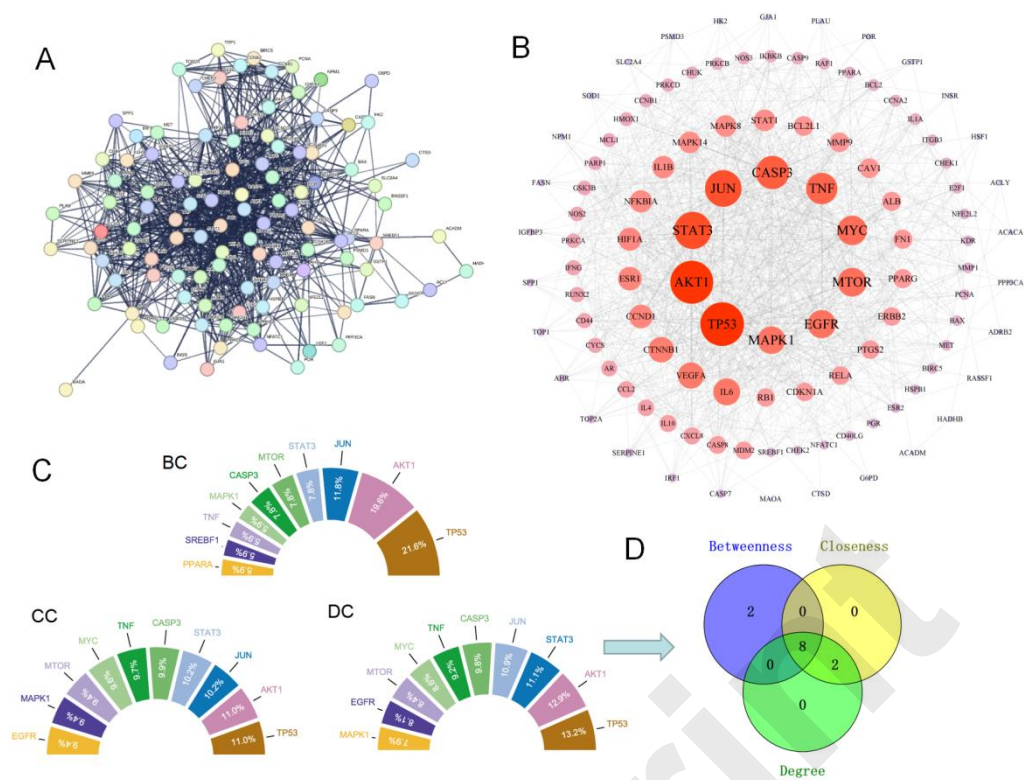


Figure 5. A: GO analysis; B: KEGG analysis; C: Drug target-pathway network.

GO: gene ontology; KEGG: Kyoto Encyclopedia of Genes and Genomes.

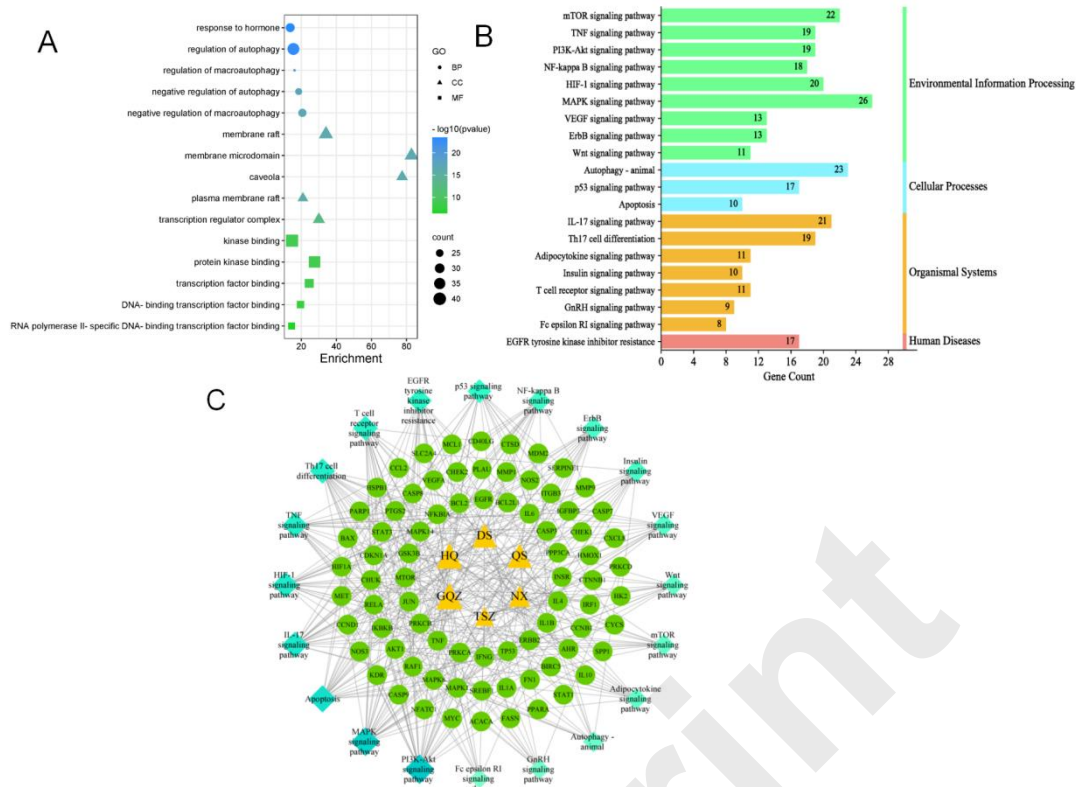


Figure 6. A: Three topology modules selected by the cytohubb plugin (2.1.2). BC, CC, and DC protein interaction networks were constructed by Cytoscape software, and core interaction networks were constructed according to the eight core targets. **B:** Significant signal pathway obtained from core target enrichment. At the same time, a three-layer circular network diagram was constructed. Different colors represent different signal pathways and enrichment targets, respectively, and node size represents the number of enriched targets. **BC:** Betweenness; **CC:** Closeness; and **DC:** Degree.

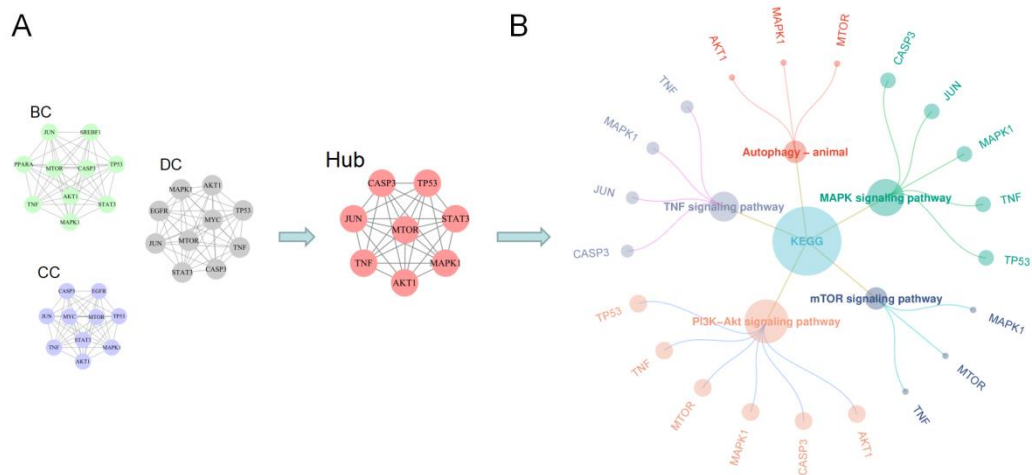


Figure 7. A: Heat map of bonding energy; B: Docking diagram of core component targets

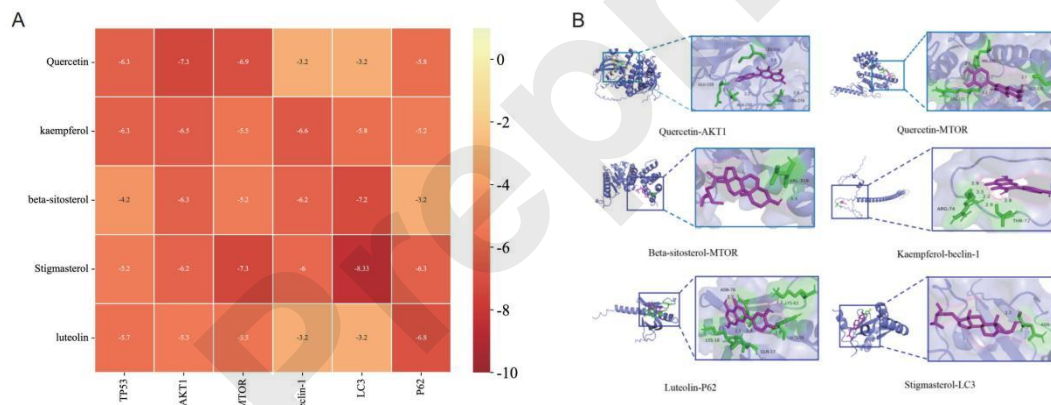
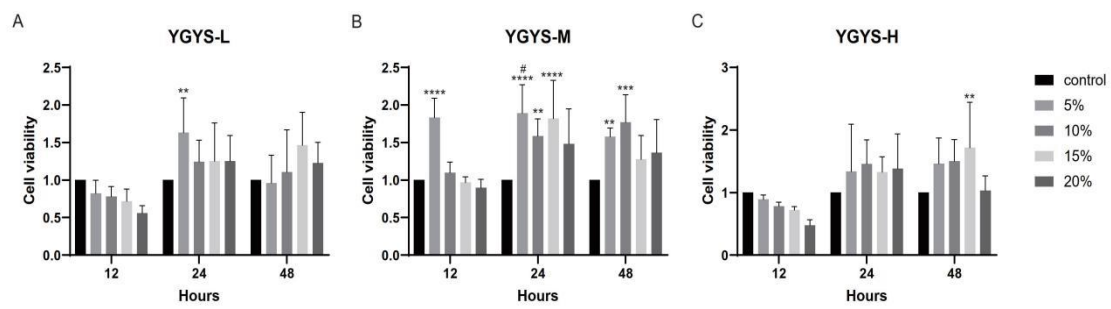


Figure 8. Effect of different concentrations of YGYSG medicated serum on the viability of MPC-5 cells assessed using the CCK-8 assay. Cells were treated with YGYS-L (A), YGYS-M (B) and YGYS-H (C) at concentrations of 5%, 10%, 15%, and 20% for 12, 24, and 48 hours.



Note: Compared with control group, ** $P < 0.01$, *** $P < 0.001$, **** $P < 0.0001$; Compared with 20%, # $P < 0.05$.

Figure 9. TEM of cells in each group.

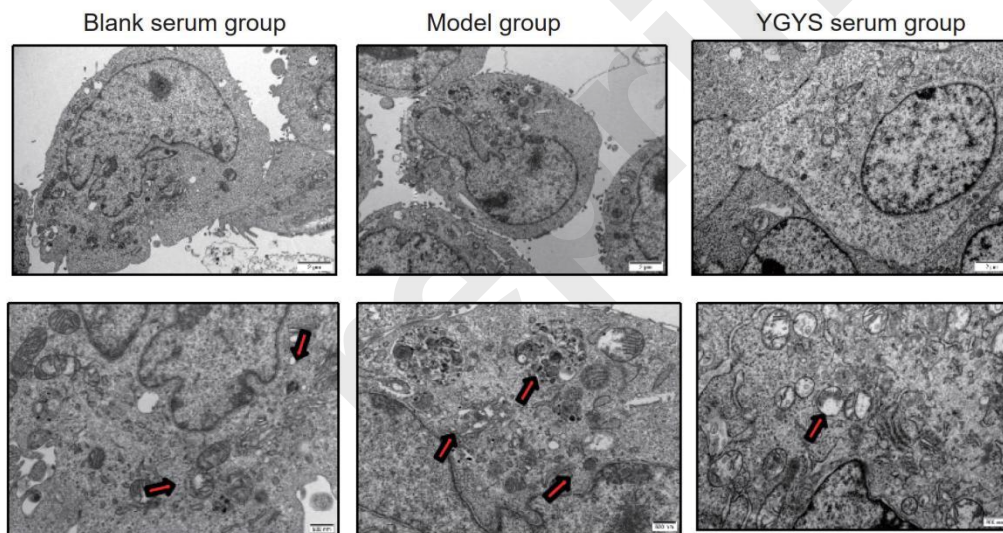
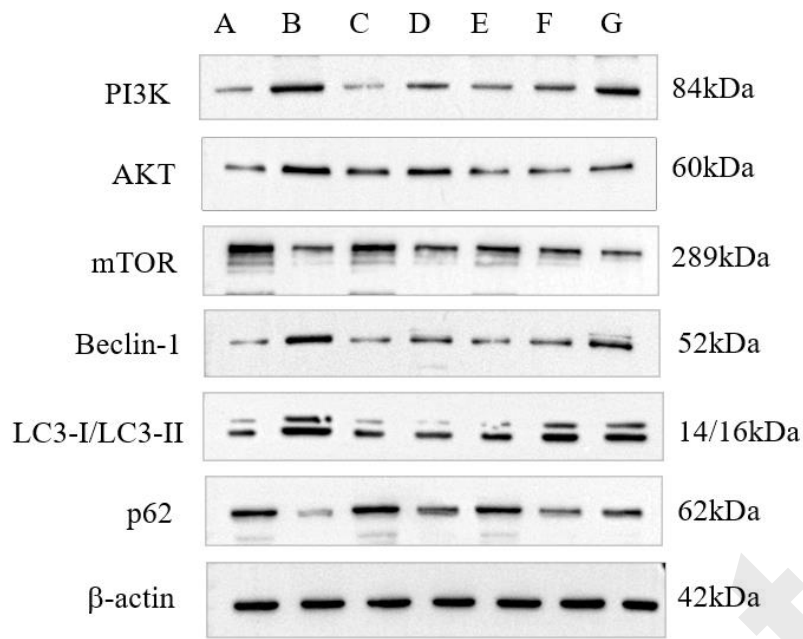
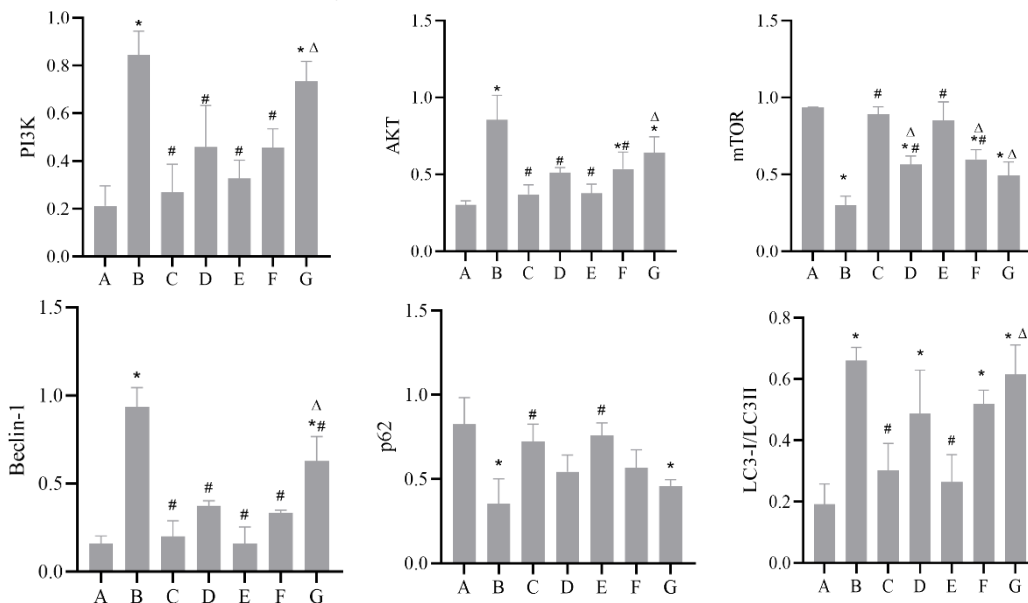


Figure 10. The protein expression of PI3K, AKT, mTOR, Beclin-1, LC3-II/LC3-I, p62 in each group.



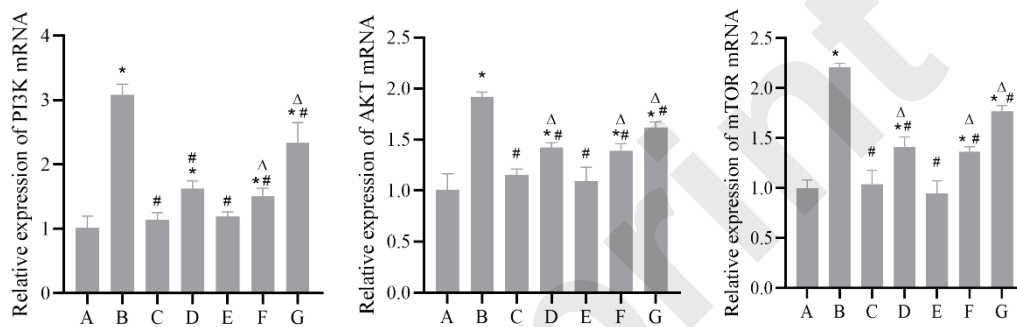
Note: A: Control group; B: Model group; C: 3-MA group; D: Benazepril group; E: YGYS-H group; F: YGYS-M group; G: YGYS-L group. Compared with control group, * $P < 0.05$; Compared with model group, # $P < 0.05$; Compared with 3-MA groups, □ $P < 0.05$.

Figure 11. Quantitative analysis of the protein expression of PI3K, AKT, mTOR, Beclin-1, LC3-II/LC3-I, p62 in each group.



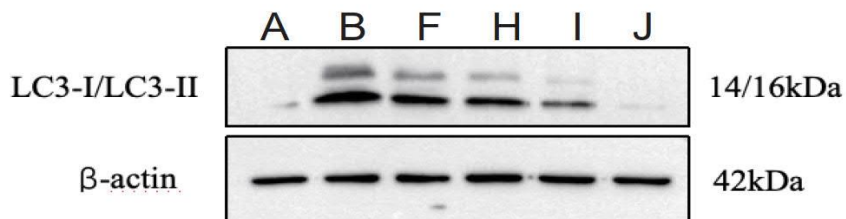
Note: A: Control group; B: Model group; C: 3-MA group; D: Benazepril group; E: YGYS-H group; F: YGYS-M group; G: YGYS-L group. Compared with control group, * $P < 0.05$; Compared with model group, # $P < 0.05$; Compared with 3-MA groups, $\nabla P < 0.05$.

Figure 12. The mRNA expression of PI3K, AKT, mTOR in each group.



Note: A: Control group; B: Model group; C: 3-MA group; D: Benazepril group; E: YGYS-H group; F: YGYS-M group; G: YGYS-L group. Compared with control group, * $P < 0.05$; Compared with model group, # $P < 0.05$; Compared with 3-MA groups, $P < 0.05$.

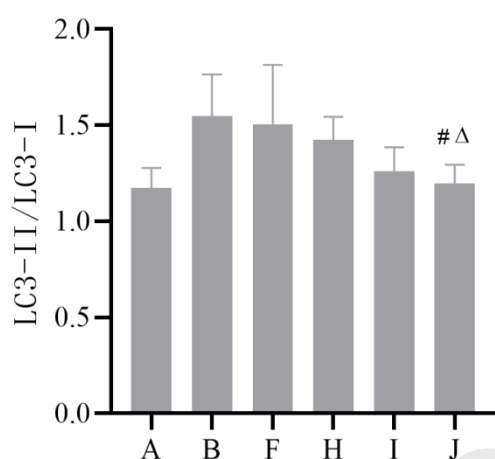
Figure 13. The protein expression of LC3-II/LC3-I in each group.



Note: A: Control group; B: Model group; F: YGYS-M group; H: YGYS-M

+3-MA(1mM) group; I: YGYS-M+3-MA(5mM) group; J: YGYS-M+3-MA(25mM) group. Compared with model group, [#] $P<0.05$; Compared with YGYS-M groups, [∇] $P<0.05$.

Figure 14. Quantitative analysis of the protein expression of LC3-II/LC3-I in each group.

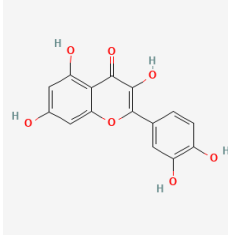
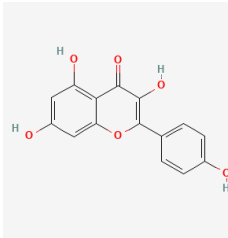
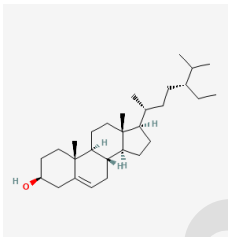
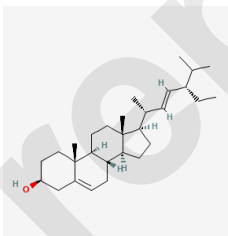
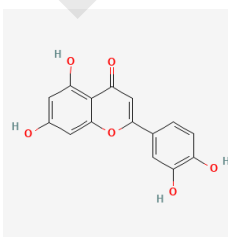
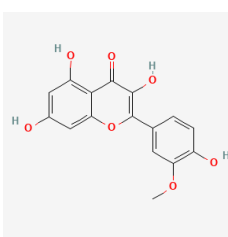


Note: A: Control group; B: Model group; F: YGYS-M group; H: YGYS-M +3-MA(1mM) group; I: YGYS-M+3-MA(5mM) group; J: YGYS-M+3-MA (25mM) group. Compared with model group, [#] $P<0.05$; Compared with YGYS-M groups, [∇] $P<0.05$.

Tables

Table 1. Ten core compounds of YGYSG in HRD treatment. YGYSG:

Yanggan-Yishui granules; HRD: hypertensive renal damage.

MOL ID	Active ingredient	Molecular structure	Molecular weight	OB%	DL	Degree
MOL0000 98	quercetin		302.23	46.43	0.28	516
MOL0004 22	kaempferol		286.24	41.88	0.24	153
MOL0003 58	beta-sitosterol 1		414.7	36.91	0.75	84
MOL0004 49	Stigmasterol		412.7	43.83	0.76	52
MOL0000 06	luteolin		286.24	36.16	0.25	50
MOL0003 54	isorhamnetin		316.26	49.60	0.31	46

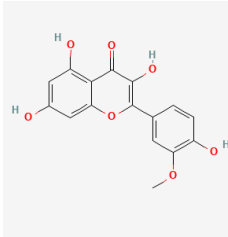
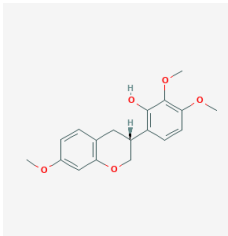
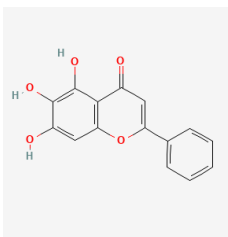
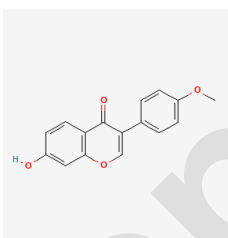
MOL0071 54	tanshinone iia		294.3	49.89	0.40	36
MOL0003 78	7-O-methylisomucronulatol		316.3	74.69	0.30	33
MOL0027 14	baicalein		270.24	33.52	0.21	31
MOL0003 92	formononetin		268.26	66.39	0.21	29

Table 2. Target information of HRD treated by YGYSG through the autophagy pathway. YGYSG: Yanggan-Yishui granules; HRD: hypertensive renal damage.

No	Gene name	Protein name	Degree
1	NOS2	Nitric oxide synthase, inducible	63
2	PTGS2	Prostaglandin G/H synthase 2	62
3	ESR1	Estrogen receptor	53
4	MTOR	Serine/threonine-protein kinase mTOR	52

5	ADRB2	Beta-2 adrenergic receptor	47
6	TP53	Cellular tumor antigen p53	44
7	RELA	Transcription factor p65	41
8	NPM1	Nucleophosmin	40
9	NFKBIA	NF-kappa-B inhibitor alpha	39
10	MYC	Myc proto-oncogene protein	38
11	MMP9	Matrix metalloproteinase-9	37
12	JUN	Transcription factor AP-1	36
13	ITGB3	Integrin beta-3	35
14	FASN	Fatty acid synthase	32
15	ECE1	Endothelin-converting enzyme 1	32
16	CDKN1A	Cyclin-dependent kinase inhibitor 1	31
17	CASP3	Caspase-3	30
18	BCL2	Apoptosis regulator Bcl-2	30
19	PDE3A	cGMP-inhibited 3',5'-cyclic phosphodiesterase A	29
20	PGR	Progesterone receptor	29
21	CCNA2	Cyclin-A2	29
22	GSK3B	Glycogen synthase kinase-3 beta	26
23	ESR2	Estrogen receptor beta	26
24	CHEK1	Serine/threonine-protein kinase Chk1	26
25	TNF	Tumor necrosis factor	25

26	STAT3	Signal transducer and activator of transcription 3	25
27	CCND1	G1/S-specific cyclin-D1	25
28	BIRC5	Baculoviral IAP repeat-containing protein 5	24
29	BCL2L1	Bcl-2-like protein 1	24
30	MAPK14	Mitogen-activated protein kinase 14	24
31	TOP2A	DNA topoisomerase 2-alpha	24
32	VEGFA	Vascular endothelial growth factor A	24
33	TOP1	DNA topoisomerase 1	23
34	SLC2A4	Solute carrier family 2, facilitated glucose transporter member 4	23
35	RB1	Retinoblastoma-associated protein	22
36	PPARG	Peroxisome proliferator-activated receptor gamma	22
37	PCNA	Proliferating cell nuclear antigen	21
38	MMP1	Interstitial collagenase	21
39	MET	Hepatocyte growth factor receptor	20
40	MDM2	E3 ubiquitin-protein ligase Mdm2	19
41	MCL1	Induced myeloid leukemia cell differentiation protein Mcl-1	19
42	MAPK1	Mitogen-activated protein kinase 1	19
43	INSR	Insulin receptor	19

44	IL6	Interleukin-6	18
45	IL4	Interleukin-4	18
46	IL10	Interleukin-10	18
47	IFNG	Interferon gamma	17
48	HMOX1	Heme oxygenase 1	17
49	GSTP1	Glutathione S-transferase P	17
50	ERBB2	Receptor tyrosine-protein kinase erbB-2	16
51	EGFR	Epidermal growth factor receptor	16
52	CD40LG	CD40 ligand	15
53	CCNB1	G2/mitotic-specific cyclin-B1	15
54	CASP9	Caspase-9	15
55	CASP7	Caspase-7	15
56	AKT1	RAC-alpha serine/threonine-protein kinase	15
57	PLAU	Urokinase-type plasminogen activator	14
58	MAOA	Amine oxidase [flavin-containing] A	14
59	PRKCA	Protein kinase C alpha type	14
60	PON1	Serum paraoxonase/arylesterase 1	14
61	MAP2	Microtubule-associated protein 2	14
62	CASP8	Caspase-8	13
63	BAX	Apoptosis regulator BAX	13
64	STAT1	Signal transducer and activator of transcription	13

		1-alpha/beta	
65	SPP1	Osteopontin	12
66	SOD1	Superoxide dismutase [Cu-Zn]	12
67	SERPINE1	Plasminogen activator inhibitor 1	12
68	RUNX2	Runt-related transcription factor 2	12
69	RASSF1	Ras association domain-containing protein 1	12
70	RAF1	RAF proto-oncogene serine/threonine-protein kinase	12
71	PSMD3	26S proteasome non-ATPase regulatory subunit 3	12
72	PRKCB	Protein kinase C beta type	11
73	PPARA	Peroxisome proliferator-activated receptor alpha	11
74	POR	NADPH--cytochrome P450 reductase	11
75	PARP1	Poly [ADP-ribose] polymerase 1	11
76	NPEPPS	Puromycin-sensitive aminopeptidase	10
77	NOS3	Nitric oxide synthase, endothelial	10
78	NFE2L2	Nuclear factor erythroid 2-related factor 2	10
79	IRF1	Interferon regulatory factor 1	9
80	IL1B	Interleukin-1 beta	9
81	IL1A	Interleukin-1 alpha	9
82	IGFBP3	Insulin-like growth factor-binding protein 3	9

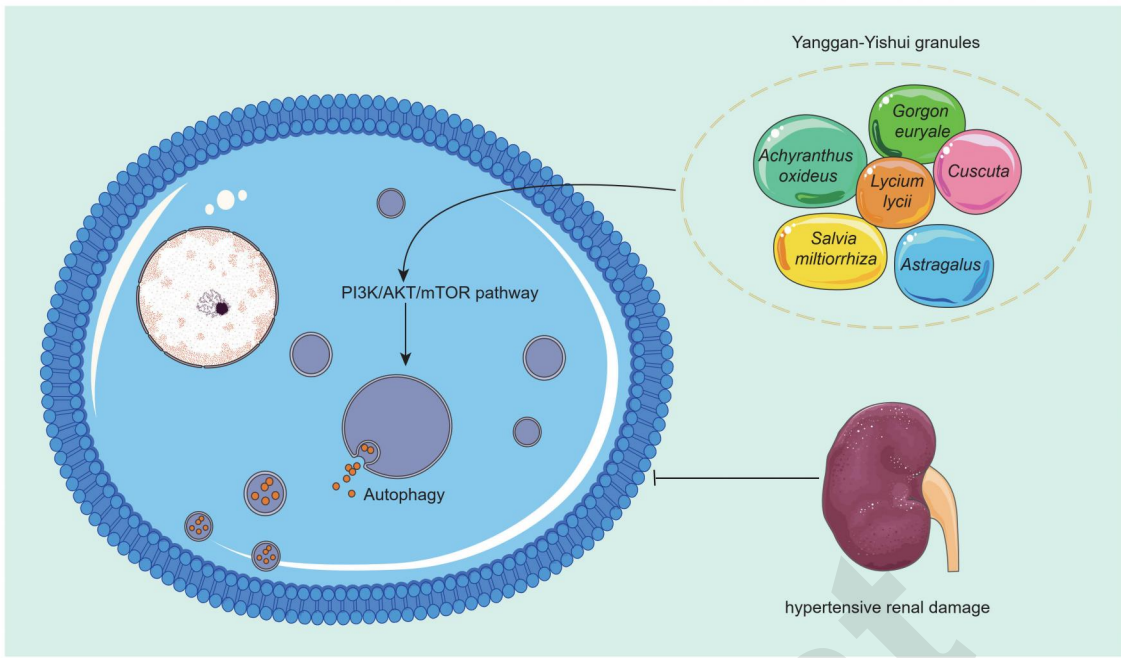
83	HSPB1	Heat shock protein beta-1	8
84	HSF1	Heat shock factor protein 1	8
85	HK2	Hexokinase-2	8
86	HIF1A	Hypoxia-inducible factor 1-alpha	7
87	GJA1	Gap junction alpha-1 protein	7
88	EIF6	Eukaryotic translation initiation factor 6	6
89	E2F1	Transcription factor E2F1	6
90	DCAF5	DDB1- and CUL4-associated factor 5	6
91	CXCL8	Interleukin-8	5
92	CTSD	Cathepsin D	5
93	CHUK	Inhibitor of nuclear factor kappa-B kinase subunit alpha	5
94	CHEK2	Serine/threonine-protein kinase Chk2	5
95	CCL2	C-C motif chemokine 2	4
96	CAV1	Caveolin-1	4
97	AHR	Aryl hydrocarbon receptor	4
98	ACACA	Acetyl-CoA carboxylase 1	4
99	PPP3CA	Serine/threonine-protein phosphatase 2B catalytic subunit alpha isoform	4
100	MAPK8	Mitogen-activated protein kinase 8	4
101	IKBKB	Inhibitor of nuclear factor kappa-B kinase	4

		subunit beta	
102	ATP5F1B	ATP synthase subunit beta, mitochondrial	3
103	KDR	Vascular endothelial growth factor receptor 2	3
104	OLR1	Oxidized low-density lipoprotein receptor 1	2
105	NFATC1	Nuclear factor of activated T-cells, cytoplasmic 1	2
106	CYCS	Cytochrome c	2
107	PRKCD	Protein kinase C delta type	2
108	FN1	Fibronectin	1
109	ALB	Serum albumin	1
110	CTNNB1	Catenin beta-1	1
111	HPSE	Heparanase	1
112	CD44	CD44 antigen	1
113	SREBF1	Sterol regulatory element-binding protein 1	1
114	HADHB	Trifunctional enzyme subunit beta, mitochondrial	1
115	G6PD	Glucose-6-phosphate 1-dehydrogenase	1
116	ACLY	ATP-citrate synthase	1
117	ACADM	Medium-chain specific acyl-CoA dehydrogenase, mitochondrial	1
118	AR	Androgen receptor	1

Table 3. Effects of different concentrations of drug-containing serum at different time points on the activity of MPC-5 cells (\pm S).

Groups	serum concentration	Time		
		12h	24h	48h
YGYS-L	5%	0.82 \pm 0.16	1.63 \pm 0.42*	0.96 \pm 0.34
	10%	0.78 \pm 0.12	1.24 \pm 0.26	1.10 \pm 0.51
	15%	0.72 \pm 0.15	1.25 \pm 0.46	1.47 \pm 0.40
	20%	0.56 \pm 0.09	1.25 \pm 0.31	1.23 \pm 0.25
YGYS-M	5%	1.83 \pm 0.23*	1.89 \pm 0.35*#	1.58 \pm 0.11*
	10%	1.20 \pm 0.13	1.58 \pm 0.21*	1.77 \pm 0.33*
	15%	0.97 \pm 0.07	1.81 \pm 0.47*	1.28 \pm 0.29
	20%	0.90 \pm 0.10	1.48 \pm 0.43	1.36 \pm 0.40
YGYS-H	5%	0.89 \pm 0.06	1.34 \pm 0.69	1.46 \pm 0.38
	10%	0.78 \pm 0.58	1.45 \pm 0.35	1.50 \pm 0.31
	15%	0.72 \pm 0.05	1.33 \pm 0.23	1.71 \pm 0.66*
	20%	0.47 \pm 0.09	1.38 \pm 0.51	1.03 \pm 0.21

Note: Compared with control group, * P <0.05; Compared with YGYS-M 24h-20% group, # P <0.05.



Preprint